Article

pubs.acs.org/Biomac

Shear and Extensional Rheology of Cellulose/Ionic Liquid Solutions

Simon J. Haward,*[,†] Vivek Sharma,[†] Craig P. Butts,[‡] Gareth H. McKinley,[†] and Sameer S. Rahatekar*[,§]

[†]Hatsopoulos Microfluids Laboratory, Department of Mechanical Engineering, Massachusetts Institute of Technology, Cambridge, Massachusetts 02139, United States

[‡]Chemical and Biological NMR Spectroscopy Group, School of Chemistry and [§]Advanced Composites Centre for Innovation & Science, Department of Aerospace Engineering, University of Bristol, University Walk, Bristol BS8 1TR, United Kingdom

Supporting Information

ABSTRACT: In this study, we characterize the shear and extensional rheology of dilute to semidilute solutions of cellulose in the ionic liquid 1-ethyl-3-methylimidazolium acetate (EMIAc). In steady shear flow, the semidilute solutions exhibit shear thinning, and the high-frequency complex modulus measured in small amplitude oscillatory shear flow exhibits the characteristic scaling expected for solutions of semiflexible chains. Flow curves of the steady shear viscosity plotted against shear rate closely follow the frequency dependence of the complex viscosity acquired using oscillatory shear, thus satisfying the empirical Cox−Merz rule. We use capillary thinning rheometry (CaBER) to characterize the relaxation times and apparent extensional viscosities of the semidilute cellulose solutions in a uniaxial extensional flow that mimics the dynamics encountered in the spin-line during fiber spinning processes. The apparent extensional viscosity and characteristic relaxation times of the semidilute cellulose/EMIAc solutions increase dramatically as the solutions enter the entangled concentration regime at which fiber spinning becomes viable.

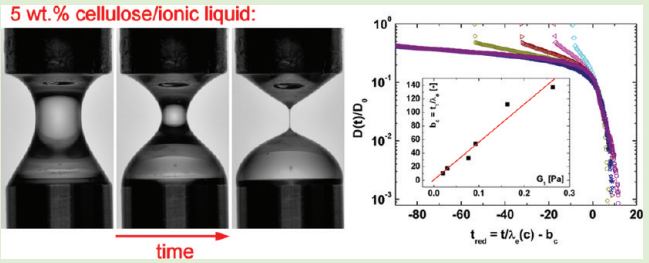

INTRODUCTION

Carbohydrate polymers or polysaccharides are some of the most abundant biomacromolecules in nature and function as energy storage materials (starch, guar gum) and as structural materials (cellulose in plants, chitin in insect exoskeletons). They find applications in industry as additives for modifying the rheology of structured, complex fluids (paints, inks, cosmetics, pharmaceuticals), on the one hand, and to provide additional reinforcing strength to fiber composites, on the other hand.[1−6] Cellulose is a carbohydrate-based linear-chain polymer generated from one to four linked β-D-anhydroglucopyranose molecules. The three hydroxyl groups per anhydroglucose unit (AGU) form hydrogen bonds that provide cellulose with the structural integrity that is critical for its biological function but also confer limited water solubility.[4] Cellulose is made water-soluble by modifying it into a cellulose ether or cellulose ester, where one, two, or three hydroxyl groups of the 1−4 linked β-D-anhydroglucopyranose building blocks are substituted by ethers or esters.[1−4] The extensive interchain and intrachain hydrogen bonds that make it difficult to dissolve unmodified cellulose in common organic solvents, or in water, are also responsible for providing cellulose with a higher degree of crystallinity, tensile strength, and other desirable properties that drive its use in textile fibers, films, nanoparticles, aerogels, or cellulose−matrix−cellulose filler composites.[4,6] Regenerated cellulose products like viscose rayon fibers or cellophane films are traditionally manufactured by using aggressive solvents like sodium hydroxide/carbon disulfide and sulphuric acid that leave a large environmental footprint.[7,8] These solvents can also cause irreversible degradation of glucosidic bonds along the cellulose chains, leading to a decrease in the molecular weight.[9] The difficulty of processing cellulose is perhaps the single most important contributor to the limited use of this most abundant, biocompatible, and biodegradable polymer.

Over the past decade, ionic liquids (ILs) have emerged as a new class of environmentally benign solvents for dissolution and processing of a number of natural polymers including cellulose,[10−13] silk,[14] keratin,[15] and chitin.[16,17] Even raw biomass such as lignocellulose (i.e., wood)[18−21] and crustacean shells[17] can be dissolved and processed into films, fibers, and other end products using ILs as solvents. ILs are potentially far less hazardous and more sustainable than the solvents traditionally used for cellulose because they have low volatility, good chemical and thermal stability, low flammability[22] and can also be recycled.[23] The aforementioned properties and also the high ionic conductivity of IL solvents are also attractive for broader applications in macromolecular science such as for use as polymerization media, in polymer gels as electrolyte matrices, for the formation of porous polymeric media, and for creating hybrid, composite materials (see the recent reviews and references therein).[24−26] Most of the traditional solvents for cellulose have a high polarity, which is favorable for disrupting the extensive inter- and intramolecular hydrogen bonds that normally limit solubility.[9] Cellulose dispersed in

Received: March 15, 2012
Revised: April 4, 2012

   dx.doi.org/10.1021/bm300407q | Biomacromolecules XXXX, XXX, XXX−XXX

highly polar ILs can potentially form electron donor−electron acceptor (EDA) complexes with the charged species of the IL, effectively making hydroxyl groups unavailable for hydrogen bonding and thus aiding in cellulose dissolution.[9] NMR studies of cellobiose solvation in the IL 1-ethyl-3-methylimidazolium acetate (EMIAc) (the IL used in the present work) indicate that hydrogen bonding takes place between the cellulose hydroxyl groups and both the EMI^+ cation and the Ac^- anion. The strongest hydrogen bonding associations are formed between the Ac^- ion and the hydroxyl hydrogen atom, whereas weaker hydrogen bonds are established between the EMI^+ ion and the hydroxyl oxygen atom.[27]

The understanding of the concentration-dependent shear and extensional rheology of cellulose dissolved in ILs is a necessary step toward realizing the potential of ILs as processing aids (especially in fiber spinning, film casting, and spraying) and also in understanding the dynamics and thermodynamics of cellulose chains dispersed in ILs. Specifically, dilute solution viscometry and the resulting intrinsic viscosity measurements provide the simplest method for assessing the pervaded hydrodynamic volume of the dispersed solute and for determining polymer solution properties such as chain flexibility, polymer−solvent interactions, and polymer−polymer interactions.[28,29] Furthermore, the characterization of the material response to applied shear deformation, as characterized by flow curves of steady shear viscosity against applied shear rate or applied shear stress, is essential for designing processing strategies.[29] Consequently, the shear rheological characterization of cellulose dissolved in ILs has received much attention in recent years.[30−37] However, the study of the extensional flow behavior of cellulose/IL solutions is very limited (only one report exists in the literature[36]), even though extensional flows that involve strong stretching of fluid elements arise in many natural and industrial processes such as printing, fiber spinning, porous media flows, extrusion, molding, coating, spraying, and so on.[38,39] The present study examines both the shear and extensional rheology of dilute to semidilute cellulose solutions in EMIAc (a room-temperature IL).

Early studies on the macromolecular nature of cellulose and cellulose derivatives by Staudinger, Mark, Kuhn, Houwink, Ostwald, Flory, and Huggins established many of the fundamental concepts concerning the relationships between solution viscosity, polymer molecular weight, and polymer−solvent interactions (solvent quality).[1,3−5,40−42] In contrast with commonly used synthetic polymers like polyolefins, poly(ethylene oxide) (PEO), or polystyrene (PS), cellulose and cellulose derivatives are characterized by a high intrinsic viscosity, large radius of gyration, and large characteristic ratio, C_∞ ($C_\infty < 10$ for most polyolefins and PEO, but $C_\infty > 10$ for many cellulose derivatives).[2,4] Cellulose and its derivatives also have a small second virial coefficient, display viscous shear thinning in semidilute and concentrated solutions, and have a large persistence length, l_p (cellulose in cadoxen has $l_p = 7$ nm, hydroxyethyl cellulose in water has $l_p = 10−30$ nm, and xanthan in water has $l_p = 50−210$ nm, whereas, by contrast, $l_p < 2$ nm for PEO and polyolefins).[2,4] These characteristics are all indications that cellulose chains adopt semiflexible conformations in solution.[2,4,5] Highly concentrated solutions of cellulose and cellulose derivatives can also form lyotropic liquid crystal phases, which can be advantageous in creating fibers, films, or composites with a higher degree of inbuilt order and advantageous mechanical properties.[2] Indeed, a number of researchers have used IL-based fiber spinning of cellulose to manufacture pure regenerated cellulose fibers[43] as well as multifunctional cellulose fibers reinforced and functionalized with, for example, carbon nanotubes,[44,45] magnetic particles,[46] and antibacterial agents.[11] As a processing aid for cellulose, economical and eco-friendly ILs have the potential to drive the latest resurgence in the use of cellulose-based fibers. The significance of the extensional properties of the biopolymer solutions characterized in this study can be best discussed using an example and is described next in the context of the dry-jet wet spinning process.

The dry-jet wet spinning process (schematically shown in Figure 1) consists of (1) extrusion of the polymer solution (spinning dope) through a die (spinneret), followed by (2) stretching of the emerging fluid jet into a filament of the desired diameter in an air gap before (3) the solvent-rich filament is immersed in a coagulation bath of a nonsolvent, where the

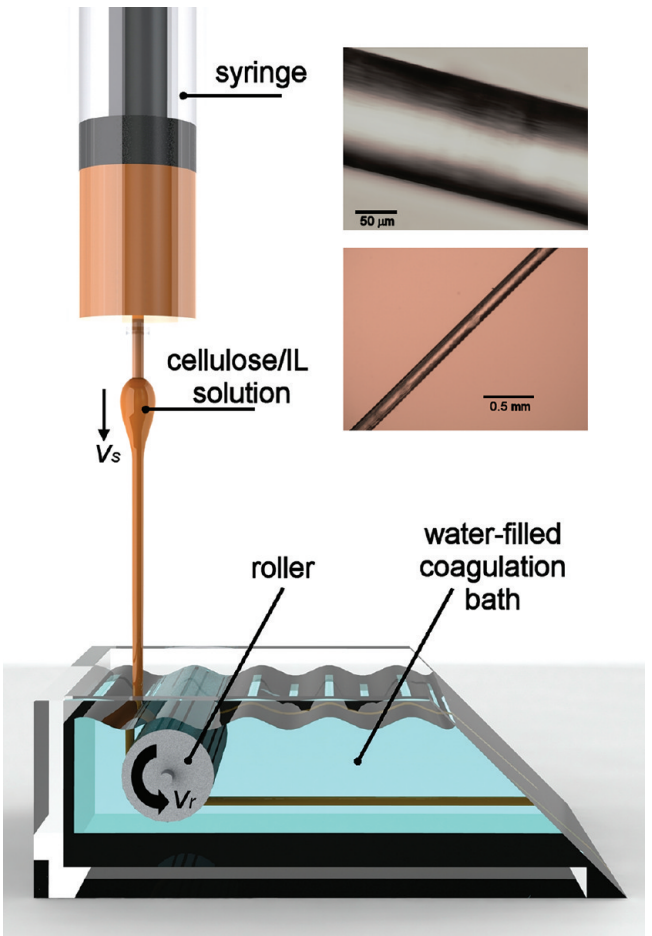

Figure 1. Schematic representation of part of the dry-jet wet spinning process. Cellulose-doped ionic liquid solution is ejected from a syringe (showing viscoelastic die-swell at the exit) and forms a stable spin-line before entering a water-filled coagulation bath. The roller rotates with a velocity v_r greater than the exit velocity of fluid from the syringe (v_s), providing a draw ratio $DR = v_r/v_s$, which enhances the extensional stress on the thinning fluid filament in the air gap and helps to align the cellulose molecules prior to coagulation. Subsequently, the coagulating filament passes around a second roller (not shown) within the water bath before being taken up on a spool as a coagulated fiber. The inset micrographs show fibers spun from an 8 wt % cellulose/ionic liquid solution with a 1 mm diameter exit die and a draw ratio of $DR = 11$.

dx.doi.org/10.1021/bm300407q | Biomacromolecules XXXX, XXX, XXX−XXX

filament becomes enriched in polymer as the miscible solvent is leached out and precipitation occurs under tension. Finally, the coagulated polymeric filament is taken up on a spool. In the case of a spinning dope composed of cellulose dispersed in a nonvolatile IL, water can be used as the nonsolvent in the coagulation bath. Because the IL has a low vapor pressure and can be separated easily from water by evaporation, the fiber spinning process produces no hazardous gaseous or liquid effluents, which are characteristic of the viscose rayon and other conventional processes. Whereas knowledge of the shear rheology of the fiber spinning solutions assists in controlling the flow rates in the extrusion process, it is the response to extensional flows that primarily controls the kinematics underlying formation of filaments and the mechanical properties of the final fiber, such as the modulus and ultimate tensile strength. A complex mixed flow with extensional and shearing components occurs first within the spinneret as fluid elements are squeezed through the exit die. Subsequently, a predominantly shear-free uniaxial extensional flow occurs within the spin-line, where there are no confining surfaces.[47] In fiber spinning, the degree of stretching applied to the fluid filament within the air gap of distance d between die and roller is quantified in terms of the draw ratio, $DR = \nu_r/\nu_s$, where ν_r is the velocity at which fiber is taken up on the spool and ν_s is the average velocity at which fluid is ejected from the die ($\nu_s = Q/\pi r_s^2$, where Q is the volume flow rate and r_s is the die radius). A high draw ratio means that fluid is subjected to a high extension rate, $\dot{\varepsilon} \approx (\nu_r - \nu_s)/d$, and a high Hencky strain, $\varepsilon_H \approx \ln(DR)$, within the air gap, and hence a greater degree of alignment and crystallinity is expected in the resulting coagulated fiber. The inset images in Figure 1 show micrographs of fibers spun from an 8 wt % solution of cellulose in the room-temperature IL EMIAc. Extrusion was from a $2r_s = 1$ mm die with $\nu_s = 0.01$ ms^{-1}, $\nu_r = 0.11$ ms^{-1}, and $d = 2.5$ cm, providing a draw ratio of $DR = 11$, Hencky strain of $\varepsilon_H \approx 2.4$, and an extensional strain rate of $\dot{\varepsilon} \approx 4$ s^{-1}.

So far, there is only one previous study of the extensional response of cellulose dispersed in ILs,[36] and we first summarize their results. Sammons et al.[36] used a capillary extrusion rheometer to estimate the extensional viscosity of cellulose in the IL 1-butyl-3-methyl imidazolium chloride (BMICl), with measurements carried out at 80, 90, and 100 °C. Hyperbolic dies of different contraction ratios were used to provide three different Hencky strains ($\varepsilon_H = 5, 6, 7$) over a range of applied strain rates 1 s$^{-1} \leq \dot{\varepsilon} \leq 100$ s^{-1} controlled by the macroscopic volume flow rate. The pressure drop across the contraction was used as a measure of the extensional stress in the fluid. However, in such a device there is also a strong shearing component that produces a significant contribution to the global measured pressure drop from which the apparent extensional viscosity is estimated. Because the cellulose solutions studied were strongly shear-thinning,[35] the pressure drop contributed by shear varies nonlinearly with the shear or extension rate.[48] Hence, the contribution of the extensional component is difficult to isolate unambiguously from the shearing contributions, and such measurements can provide an unreliable estimate of the apparent extensional viscosity of such fluids. The capillary extrusion rheometer gives a close approximation to the flow through the die in a dry-jet wet spinning process; however, this does not correspond to the uniaxial elongational kinematics characterizing the filament deformation in the air gap prior to fiber coagulation. This is where the majority of the cellulose chain alignment is likely to take place, and where the thinning dynamics and spinning process is effectively dictated by an interplay between capillary, viscous, inertial, and elastic stresses. This stretching of material elements just outside the spinneret or die can be reproduced by the kinematics realized in the capillary breakup extensional rheometer (CaBER), as described in the present contribution.

In this study, we first characterize the rheological response of cellulose/EMIAc solutions under steady shear using standard cone-and-plate rheometry. We evaluate the intrinsic viscosity and concentration dependence of the shear viscosity and find reasonable agreement with previously published data on similar fluids.[33,44,49] The frequency dependence of the storage and loss moduli in small-amplitude oscillatory shear flow displays the characteristic scaling expected for solutions of semiflexible polymer chains. We next characterize the extensional rheology of semidilute cellulose solutions using CaBER. The CaBER instrument imposes an axial stretching deformation on a discrete cylindrical volume of test fluid placed between circular parallel plates and provides a close approximation to a shear-free purely uniaxial extensional flow.[50] The subsequent capillary thinning of the unstable liquid bridge is resisted by inertial and viscous forces and by an additional elastic contribution from the extensional deformation of the underlying fluid microstructure. Measurement of the midpoint diameter of the stretched fluid filament as it decays over time enables the determination of the instantaneous accumulated Hencky strain (ε_H), the fluid's longest relaxation time (λ_e), and the corresponding transient extensional viscosity (η_E). The transient extensional viscosity provides a rheological measure of the degree of strain hardening and the viscoelastic contribution to the total tensile force in the filament, which in turn is related to the technologically important effective material property known as "spinnability" or the ability to spin filaments or fibers from a given complex fluid.[51,52]

MATERIALS AND METHODS

Test Fluids. The IL used in this study was EMIAc, which was obtained from Sigma-Aldrich Company and produced by BASF (lot number STBB7092). The manufacturer's certificate of analysis indicates a purity of >95% and a water content of <0.3%. We performed our own ^{1}H NMR spectroscopy (500 MHz) on a sample of ~20 mg of EMIAc dissolved in 0.7 mL of $CDCl_3$ using a VNMRS500 NMR spectrometer. After phase and baseline correction (using a polynomial fit), the purity of the EMIAc was assessed by measuring the total integral regions of EMIAc versus all other unassigned peaks. Our analysis confirms the purity of the sample at >95% and suggests that there is little acetic acid composition (<2%), with the remainder made up of minor organic impurities appearing to originate from the starting materials for synthesis, for example, methylimidazole, ethyl halides, and so on. An example of an ^{1}H NMR spectrum obtained from our EMIAc sample is provided in Figure S1 of the Supporting Information. The water content in the EMIAc sample was 0.21 wt %, as assessed by Karl Fischer titration. The EMIAc was used as received and without further purification.

The cellulose, with a degree of polymerization (DP) of 860, was provided by Rayonier (Fernandina Beach, United States). The cellulose pulp sheets were finely chopped before being dissolved in EMIAc by heating at 90 °C for 1 h with magnetic stirring. Solutions were prepared at cellulose concentrations 0.1 wt % < c < 8 wt %, and all solutions appeared transparent and homogeneous when cooled to room temperature.

Degradation of cellulose in ILs as solvents can affect the measurement of fluid rheological properties and is therefore of concern in the present study. Previous research has shown that cellulose dissolved in chloride-based ILs can undergo significant degradation when heated above 100 °C for extended periods of

time.[53−55] Degradation of cellulose in ILs can also be severe when combined with solid catalysts such as styrene-divinylbenzene resins functionalized with sulfonic groups,[56] Dowex 50WX8,[57] and trifluoroacetic acid[58] or using a combination of an acidic IL, 1-(1-propylsulfonic)-3-methylimidazolium chloride, and *p*-toluenesulphonic acid.[59] Cellulose dissolved in EMIAc has been shown to undergo modest degradation during the dissolution process[60] and also when heated above 95 °C for 8 h.[7] Although the dissolution time for our cellulose/EMIAc solutions was significantly less than this (1 h at 90 °C), we cannot discount the possibility of moderate cellulose degradation occurring during the dissolution step in our solution preparation.[60] To investigate potential degradation concerns, we have performed room-temperature rheological characterization of cellulose/EMIAc solutions over extended periods of time, which show that there is negligible change in the fluid viscosity over a 48 h interval. (See Figure S2 in the Supporting Information.) This strongly indicates that cellulose degradation following dissolution and subsequent cooling of the cellulose solution is minimal over this time period. Because the time interval between solution preparation and testing in our experiments was typically <2 h and measurements using the cone-and-plate and capillary breakup rheometers take just a few minutes or less, any effect of cellulose degradation on our rheological measurements over characteristic measurement time scales can safely be neglected.

Cone-and-Plate Shear Rheometry. The linear and nonlinear shear rheology was assessed using an AR-G2 cone-and-plate rheometer with a 40 mm diameter 2° cone. Because ILs are hygroscopic and the absorption of atmospheric water can result in precipitation of cellulose or coagulation of cellulose solutions, a thin film of light silicone oil was applied around the outer radial edge of the platens to prevent contact of the test fluid with air. The effect of this oil film on the measured rheological properties was assessed by testing pure IL with and without the applied oil film and was found to be negligible.

Capillary Breakup Extensional Rheometry. The extensional properties of cellulose/IL solutions were assessed using a CaBER (Cambridge Polymer Group) to impose a predominantly uniaxial extensional deformation to the fluid samples. This instrument enables the assessment of the longest relaxation times and extensional stresses of viscoelastic fluids through the monitoring of the capillary thinning and breakup dynamics of a fluid thread connecting two circular end plates.[61] The device has been recently used to study the extensional rheology of aqueous silk/PEO solutions in relation to their electrospinning properties[62] as well as the extensional properties of dilute to semidilute polysaccharide solutions[63] and associating polymer solutions.[64] The CaBER device uses an initially cylindrical volume of fluid ($V \approx 0.06$ mL), which forms a liquid bridge between circular parallel plates of diameter $D_0 = 6$ mm and initial separation $L_0 = 2$ mm (initial aspect ratio $\Lambda_0 = L_0/D_0 = 0.33$). To minimize gravitational sagging and obtain an approximately cylindrical liquid bridge, we chose the initial separation to be less than the capillary length $l_{cap} = (\sigma/\rho g)^{1/2}$, where σ is the IL surface tension, $\rho = 1.027$ g cm^{-3} is the IL density, and $g = 9.81$ m s^{-2} is the acceleration due to gravity.[65] The surface tension of the EMIAc was measured to be $\sigma = 47$ mN m^{-1} using a Krüss K10ST digital tensiometer, resulting in $l_{cap} \approx 2.2$ mm.

At time $t_0 = -50$ ms, the top end plate was displaced upward following an exponential profile $L(t) = L_0 e^{\dot{\varepsilon}_0(t-t_0)}$ to achieve a final plate separation of $L_f = 6$ mm at time $t = 0$ s (final aspect ratio $\Lambda_f = L_f/D_0 = 1.0$). The subsequent evolution of the liquid filament diameter ($D(t)$) was monitored at the midplane between the end plates (i.e., at $L = L_f/2$) using a laser micrometer. The dynamics of the liquid bridge thinning and breakup process were also recorded at 60 frames per second using a 6 megapixel CCD camera (Casio Exilim EX-F1), with a resolution of ~7 μm/pixel.

For a purely viscous liquid of viscosity η_s and surface tension σ, the midplane diameter is found to decrease linearly with time according to[38,66]

$$D(t) = 0.0709\frac{2\sigma}{\eta_s}(t_c - t) \tag{1}$$

where t_c is the capillary breakup time and the numerical prefactor is found from the solution for the self-similar shape of the decaying viscous filament.[67] For a polymer solution, the liquid bridge initially drains under a predominantly capillary-driven flow that is resisted by the viscous stress arising from the solvent. As a result of the extensional flow generated during the thinning of the liquid filament, the deformation of the underlying microstructure results in an additional elastic stress that grows with increasing strain and ultimately dominates the viscous stress from the solvent. This marks the onset of an elastocapillary thinning regime,[68] and a retardation in the time to eventual breakup. In the elastocapillary regime, the transient extensional properties of the fluid can be determined by measuring the rate of evolution in the midfilament diameter and by using the balance between elastic and capillary forces, as described in eqs 2−6 below.

For a model viscoelastic fluid in the elastocapillary thinning regime the midplane diameter of the filament decays exponentially as[38,50]

$$\frac{D(t)}{D_0} \approx \left(\frac{G_1 D_0}{4\sigma}\right)^{1/3} \exp[-t/3\lambda_e] \tag{2}$$

where G_1 is related to the elastic modulus and λ_e is the longest fluid relaxation time, both of which will vary with cellulose concentration. For a cylindrical fluid filament, we can define the instantaneous strain rate ($\dot{\varepsilon}$) and the accumulated Hencky strain (ε_H) as follows[50,68]

$$\dot{\varepsilon}(t) = -\frac{2}{D(t)}\frac{dD(t)}{dt} \tag{3}$$

$$\varepsilon_H(t) = \int_0^t \dot{\varepsilon}(t)\, dt = 2\ln\left(\frac{D_0}{D(t)}\right) \tag{4}$$

The axial force balance on the fluid column is given by

$$\Delta\tau(t) = 3\eta_s\dot{\varepsilon}(t) + (\tau_{zz} - \tau_{rr}) = \frac{2\sigma}{D(t)} \tag{5}$$

where $2\sigma/D(t)$ is the capillary pressure driving the filament thinning process and $\Delta\tau(t)$ is the total extensional stress difference in the elongating filament.

Combining eqs 3 and 5, the apparent transient extensional viscosity of the stretching fluid can then be evaluated using the following expression

$$\eta_E = \frac{\Delta\tau(t)}{\dot{\varepsilon}(t)} = -\frac{\sigma}{dD(t)/dt} \tag{6}$$

Because the flow in the CaBER instrument is essentially shear-free, we define the Trouton ratio as the ratio of extensional viscosity to the zero-shear viscosity of the solution; that is, $Tr = \eta_E/\eta_0$. For Newtonian fluids in uniaxial extensional flow, the expected Trouton ratio is $Tr = 3$.

RESULTS

Shear Rheology. In Figure 2, we show the steady shear viscosity $\eta(\dot{\gamma})$ as a function of the shear rate $\dot{\gamma}$ and the complex viscosity $\eta^*(\omega)$ as a function of the angular frequency ω for cellulose solutions over a range of concentrations. For each concentration, the steady shear viscosity overlays the complex viscosity very well, indicating that the empirical Cox−Merz rule[69] (which states that $|\eta^*(\omega)| \cong \eta(\dot{\gamma})|_{\dot{\gamma}=\omega}$) holds very well for these IL-based solutions. The pure EMIAc solvent has a viscosity of $\eta_s \approx 0.1$ Pa·s at 25 °C, which is invariant with shear rate. This is in excellent agreement with previous measurements made on well-characterized EMIAc samples, confirming the high purity and low water content of our IL solvent.[70,71] The approximate Arrhenius relationship between viscosity and temperature for EMIAc and cellulose solutions and their activation energies have been reported previously by Gericke et al.[33] As the cellulose concentration is increased, the zero-shear-

dx.doi.org/10.1021/bm300407q | Biomacromolecules XXXX, XXX, XXX−XXX

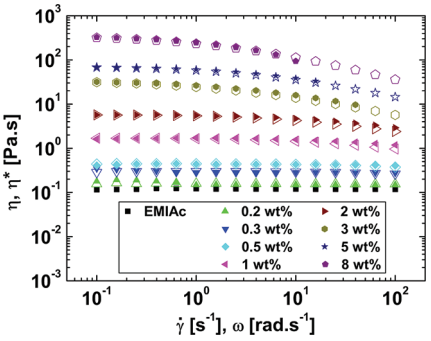

Figure 2. Viscosity as a function of shear rate (filled symbols) and complex viscosity as a function of angular frequency (hollow symbols) for cellulose/EMIAc solutions at 25 °C and the concentrations indicated.

rate viscosity increases by almost four orders of magnitude and the solutions become progressively more shear-thinning, as has been observed by various authors for cellulose dissolved in ILs[31,33,35,37,44,49] and for polysaccharides in general when the concentration is raised.[4,5]

In Figure 3a, we show the zero-shear-rate viscosity (η_0) as a function of the cellulose concentration. We observe a linear region at dilute cellulose concentrations (c < 0.5 wt %), followed by a power law dependence, $\eta_0 \propto c^n$, for c > 0.5 wt %. For 0.5 wt % ≤ c ≤ 8 wt %, the power law scaling of η_0 for our cellulose sample at 25 °C has an exponent of ∼2.4, which is

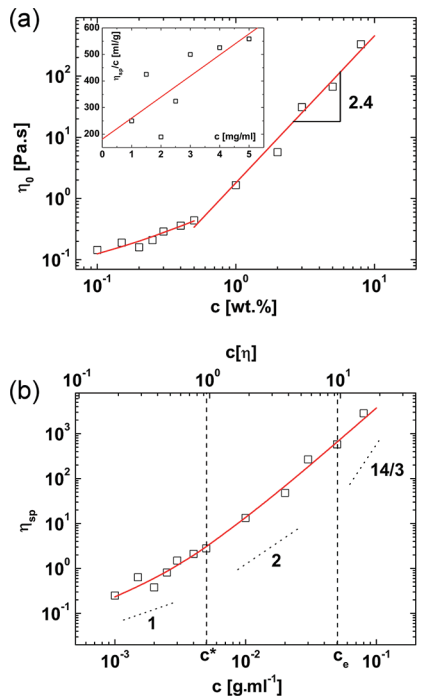

Figure 3. (a) Zero-shear-rate viscosity as a function of cellulose concentration. Inset: the reduced viscosity, η_{sp}/c, as a function of cellulose concentration in the dilute regime, fitted with a straight line of y intercept $[\eta]$ = 181 mL g^{-1}. (b) Specific viscosity as a function of concentration fitted with eq 7 (solid red line) and showing the estimated overlap concentration, c^*, and entanglement concentration, c_e. The straight lines of slope 1, 2, and 14/3 indicate the theoretical concentration scaling of the specific viscosity expected in the dilute, semidilute unentangled, and semidilute entangled regimes, respectively.

rather lower than some previous reported scalings for cellulose solutions at a similar temperature in the same IL solvent.[33,49] The scaling that we observe for 0.5 wt % ≤ c ≤ 8 wt % is roughly consistent with that expected in the semidilute unentangled regime.[72] The inset of Figure 3a shows the reduced viscosity (η_{sp}/c) as a function of concentration, in the dilute concentration regime, together with a linear regression. Although the reduced viscosity shows some scatter, extrapolating the linear fit to c = 0 gives a reasonable value for the intrinsic viscosity of $[\eta]$ ≈ 181 mL g^{-1}, close to previous reports for cellulose of similar DP in EMIAc (discussed in detail later).[33] We also checked this measurement using the methods described by Kulicke and Kniewske[73] and employed by Sescousse et al.[49] for cellulose/EMIAc solutions. In Figure 3b, we plot the specific viscosity η_{sp} as a function of c (and $c[\eta]$) over the entire range of tested concentrations. The data can be fitted with the polynomial expansion proposed by Kulicke and Kniewske:[73]

$$\eta_{sp} = c[\eta] + K_H(c[\eta])^2 + A(c[\eta])^n \quad (7)$$

where K_H is the Huggins coefficient and A and n are fitting parameters. Because it has been shown that EMIAc is close to a theta solvent for cellulose at room temperature,[33] the value of the Huggins coefficient was taken to be K_H = 0.5. The values obtained for $[\eta]$, A, and n from fitting the data were 188.4 mL g^{-1}, 1.905, and 2.56, respectively. Our value for $[\eta]$ is very close to the value of $[\eta]$ = 178 mL g^{-1} reported by Gericke et al. for a cellulose of similar molecular weight (DP = 1000) in EMIAc at 20 °C.[33]

Also, in Figure 3b, we indicate the approximate overlap concentration (c^* = 0.5 wt %, or 0.005 g mL^{-1}) and entanglement concentration ($c_e \approx 10 \times c^*$ = 5 wt %).[72] For a neutral polymer in a theta solvent, the scaling predictions give slopes of 1, 2, and 14/3 in the dilute, semidilute unentangled, and semidilute entangled regimes, respectively.[72,74] Although our data do not perfectly follow these trends, the agreement is reasonably close, although the lack of data at concentrations c > 8 wt % precludes a proper determination of the scaling in the entangled regime. For our particular cellulose sample of DP 860, we find that preparation of solutions in EMIAc at concentrations substantially above 8 wt % (or 0.08 g mL^{-1}) is extremely difficult and results in inhomogeneous and cloudy samples. Whereas various previous authors have achieved higher concentrations of cellulose dissolved in EMIAc,[7,11,75] up to 18 wt % in one particular example,[75] we note that these studies were performed using celluloses of lower DP than in the present work. The higher DP of our cellulose sample results in greater viscosification for a given cellulose concentration and hence restricts the maximum concentration that can be achieved because magnetic stirring becomes impossible. We can dissolve higher concentrations of high DP cellulose using a high-shear mixer; however, this method results in degradation of cellulose chains and hence a lowering in the average DP, which is undesirable.

We can use our value of $[\eta]$ to obtain an estimate of the radius of gyration R_g using the formula $R_g^2 = (1/6)\cdot([\eta]M/\Phi)^{2/3}$, where M is the cellulose molecular weight ($M \approx 140$ kDa for cellulose of DP = 860) and $\Phi = 2.8 \times 10^{23}$ mol is the Flory constant.[33,76,77] We obtain a value of $R_g \approx 18.6$ nm, which, in turn, allows an estimate of the root-mean-squared end-to-end length at equilibrium, $\langle r_0^2\rangle^{1/2} = \sqrt{6}R_g \approx 46$ nm. Assuming that EMIAc is a theta solvent for cellulose at room temperature (as

dx.doi.org/10.1021/bm300407q | Biomacromolecules XXXX, XXX, XXX−XXX

has been shown by Gericke et al.[33]), we can also estimate the length K of a Kuhn segment required to obtain such a radius of gyration from a 3D random walk: $K = \langle r_0^2 \rangle / L_C$, where $L_C \approx$ 443 nm is the contour length of the DP = 860 cellulose molecule, taking the length of a single AGU repeat unit to be l_{AGU} = 0.515 nm.[78] This gives $K \approx 4.8$ nm or $K \approx 9 l_{AGU}$. In addition, we can estimate the overlap concentration of the cellulose solutions using $c^* = M/(8N_A R_g^3)$,[79] which gives a value $c^* \approx 0.45$ wt %. This value for c^* agrees very well with the concentration at which the viscosity dependence changes from linear to a power law, as observed in Figure 3a, suggesting that the assumption of EMIAc being a theta solvent for cellulose is in fact reasonable. Finally, we note that the ratio of contour length to root-mean-squared end-to-end length is quite modest, $L_C/\langle r_0^2 \rangle^{1/2} \approx 10$, showing that only very low strains are required to completely extend this semiflexible macromolecule.

In Figure 4, we present the storage (G') and loss (G'') moduli as a function of the angular frequency, from oscillatory shear

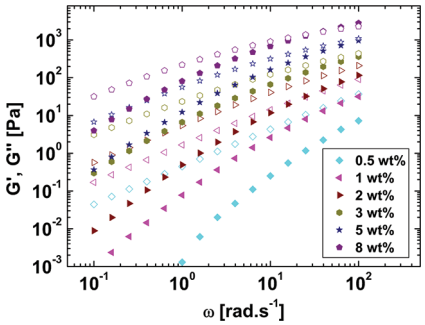

Figure 4. Storage (G', filled symbols) and loss (G'', hollow symbols) moduli as a function of angular frequency for solutions of cellulose in EMIAc at 25 °C.

tests with cellulose/EMIAc solutions in the semidilute regime measured in the AR-G2 rheometer. At lower cellulose concentrations, G'' is much greater than G', indicating viscously dominated behavior; however, for $c \geq 3$ wt %, G' approaches G'' at high frequencies. At $c = 8$ wt %, crossover is achieved for $\omega \approx$ 30 rad s^{-1}, indicating the onset of a dominant elastic response in the material. As shown in Figure 5, the oscillatory shear data are self-similar and can be superimposed on a master curve by

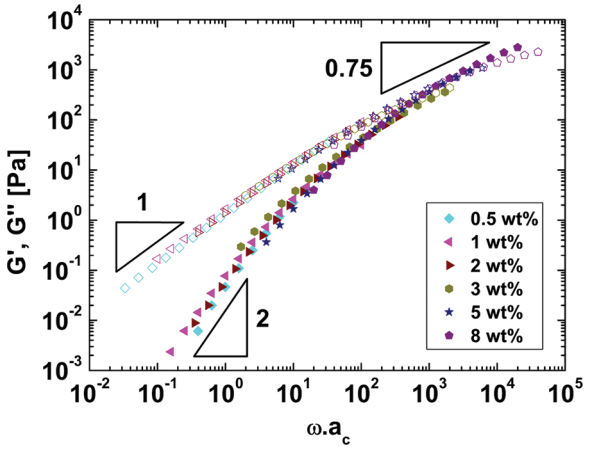

Figure 5. Master curve of the storage modulus (G', filled symbols) and loss modulus (G'', hollow symbols) as a function of reduced angular frequency $\omega_r = \omega a_c$, where a_c is a concentration-dependent shift factor.

scaling the frequency axis by a concentration-dependent factor, a_c.[80] In the terminal region, we observe the scaling $G' \sim \omega^2$ and $G'' \sim \omega$, expected for viscoelastic liquids. At high frequencies, both G' and G'' appear to approach a scaling of $\omega^{3/4}$, consistent with that expected for entangled networks of semiflexible polymers,[81,82] which suggests that the most concentrated solutions are approaching an entangled state. This would be roughly consistent with the entanglement concentration being $c_e \approx 5$ wt % or $c_e \approx 10 \times c^*$, as described by Colby.[72] In Figure 6, we plot the shift factor (a_c), found from superimposing the

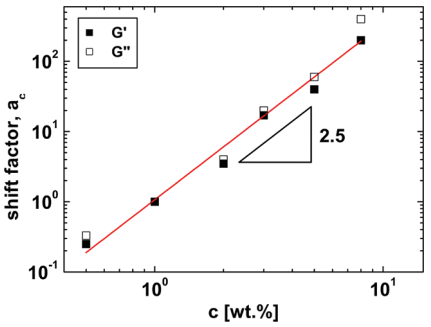

Figure 6. Shift factor (a_c) as a function of cellulose concentration in the semidilute regime, showing a power law dependence.

linear viscoelastic data, as a function of concentration. We observe a power-law dependency with an exponent of 2.5, close to that found for the zero-shear-rate viscosity over the same concentration range, and also close to the value of n found by fitting eq 7 to the specific viscosity data shown in Figure 3b.

Capillary Breakup Extensional Rheometry. In Figure 7, we present still images depicting the capillary thinning process in the pure EMIAc solvent and a few representative cellulose/IL solutions. The liquid bridge of the purely viscous solvent thins rapidly and ruptures within 0.1s, as shown in Figure 7a. The addition of 0.5 wt % of cellulose to the solution (Figure 7b) significantly retards the initial thinning dynamics, due to the increase in viscosity, and leads to the formation of a slender and axially uniform elastic filament before the final breakup (see, e.g., Figure 7b at $t/t_c = 0.72$). Further increasing the cellulose concentration to 1 and 5 wt % (Figure 7c,d, respectively) leads to progressively slower initial viscous draining dynamics and a delayed onset of the elastocapillary thinning regime (compare, for example, Figure 7b–d at t/t_c = 0.48).

Although the elastocapillary thinning regime represents only a small portion of the entire thinning dynamics prior to the eventual rupture of the filament, for each fluid it is possible to identify an exponentially decaying region on plots of the measured filament diameter versus time, as shown in Figure 8a. We denote the time at the onset of the elastocapillary regime as $t_1(c)$, which we determine from the point of intersection between the exponential fit in the elastocapillary regime and a fit to the linearly decaying, viscosity-dominated, section of the curve at earlier times (see eq 1). For times $t > t_1(c)$, the elastocapillary thinning regime is accurately described by a single exponential decay in the midpoint radius of the form

$$\frac{D(t)}{D_0} = \left(\frac{G_1 D_0}{4\sigma}\right)^{1/3} \exp[-(t - t_1(c))/3\lambda_e(c)] \quad (8)$$

By fitting this expression to the capillary-thinning data for times $t > t_1$, we can extract the relaxation time (λ_e) characterizing the

dx.doi.org/10.1021/bm300407q | Biomacromolecules XXXX, XXX, XXX–XXX

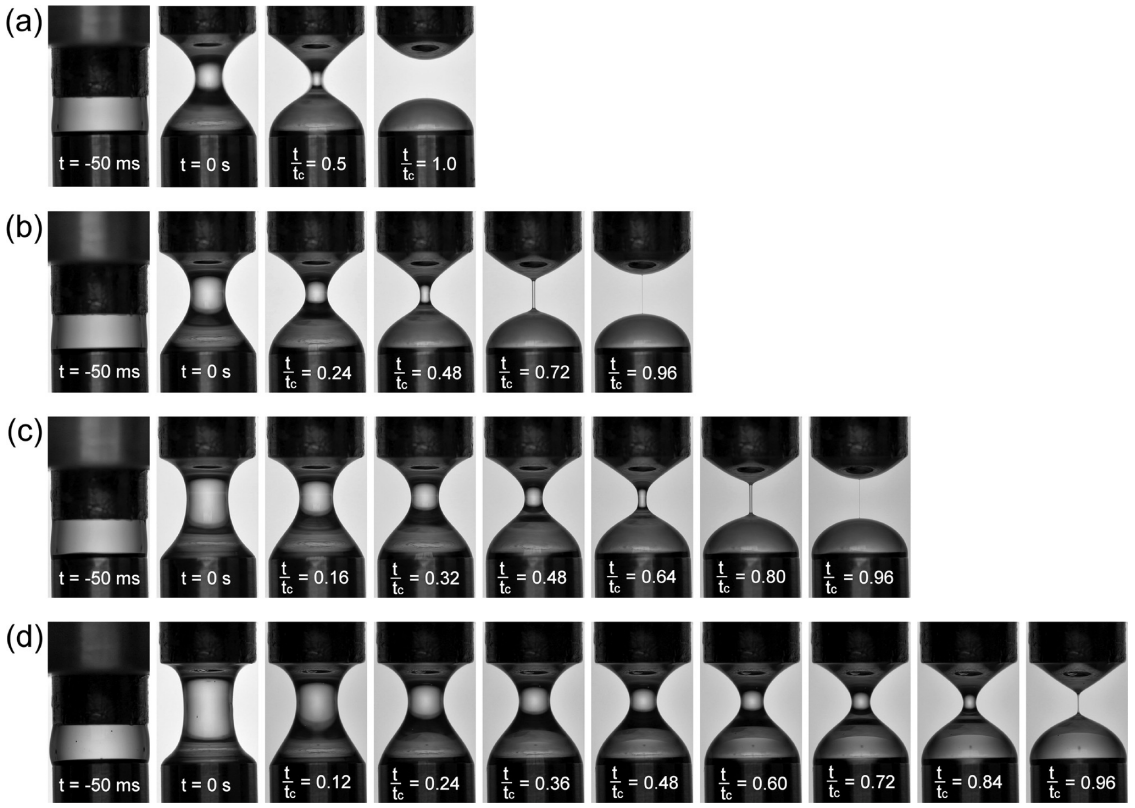

Figure 7. Still images of the capillary thinning of cellulose/IL solutions in the CaBER: (a) EMIAc, t_c = 0.07 s; (b) 0.5 wt % cellulose (c/c^* = 1, t_c = 0.56 s); (c) 1.0 wt % cellulose (c/c^* = 2, t_c = 1.7 s); and (d) 5.0 wt % cellulose (c/c^* = 10, t_c = 48.5 s). The initial gap between end plates was L_0 = 2 mm and the final gap L_f = 6 mm, giving initial and final aspect ratios of Λ_0 = 0.33 and Λ_f = 1, respectively, with plates of 6 mm diameter.

onset of chain stretching in each of these semidilute or entangled fluids. The values for $t_1(c)$ and $\lambda_e(c)$ obtained by this method are provided in Table 1.

In Figure 8b, we show how, for times greater than the elastocapillary onset time, $t_1(c)$, appropriate rescaling of the diameter and time axes allows the raw CaBER data to be collapsed onto a master curve. The diameter axis is nondimensionalized simply by dividing $D(t)$ by the initial filament diameter, D_0. The time axis is nondimensionalized by scaling with the concentration-dependent relaxation time (λ_e) and is then shifted by the concentration-dependent shift factor $b_c = t_1(c)/\lambda_e(c)$, to construct a dimensionless reduced time variable $t_{red} = t/\lambda_e(c) - t_1(c)/\lambda_e(c)$. The reduced time t_{red} = 0 marks the onset of the elastocapillary regime, and the diameter versus time curves overlay well for reduced times $t_{red} > 0$. At a reduced time of t_{red} = 0, eq 8 reduces to the following form:

$$D(t_{red} = 0) \approx D_0\left(\frac{G_1 D_0}{4\sigma}\right)^{1/3} \quad (9)$$

and the characteristic elastic modulus $G_1(c)$ of the fluid during elastocapillary thinning can be evaluated simply by rearrangement. We find that both the shift factor $b_c = t_1(c)/\lambda_e(c)$ and the characteristic modulus $G_1(c)$ increase with the concentration of cellulose in solution and that b_c scales linearly with $G_1(c)$, as shown by the insert in Figure 8b.

The relaxation times (λ_e) of the different cellulose/EMIAc solutions reported in Table 1 are also shown graphically in Figure 9, together with error estimates corresponding to the standard deviation from three such measurements. For the lowest four concentrations of cellulose examined here (see Table 1), the measured relaxation times are in the range of 30−80 ms and increase only slightly with concentration. However, for c > 3 wt % (i.e., as the semidilute cellulose solutions start to become entangled), there is a significant increase in relaxation time up to $\lambda_e \approx$ 1.7 s at c = 8 wt %, which we note is a cellulose concentration at which fibers can be spun by dry-jet wet spinning.[44] Shenoy et al. have extensively investigated the role of chain entanglement on fiber formation during electrospinning of polymer solutions and conclude that a minimum "entanglement number in solution" of $n_{e,soln}$ = 3.5 is necessary for the formation of continuous, uniform fibers.[83] For $2 \le n_{e,soln} \le 3.5$, fibers could be formed only intermittently, whereas $n_{e,soln} \approx 2$ marked a transition to spraying of droplets. Horinaka et al. have reported entanglement molecular weights, $M_{e,soln}$, for various concentration solutions of cellulose in the IL 1-butyl-3-methylimidazolium chloride (BMICl).[30] Assuming the density of cellulose to be ρ_c = 1 g cm^{-3}, they extrapolated their data to a concentration of c = 1 g cm^{-3} to obtain a value of $M_e \approx$ 3200 g mol^{-1} for a cellulose "melt". The entanglement number in solution can be determined using $n_{e,soln} = (\phi_c M)/M_e$, where ϕ_c is the volume fraction of cellulose.[83] Again assuming the same value for the cellulose density of ρ_c = 1 g cm^{-3}, we obtain values for the entanglement number of $n_{e,soln} \approx$ 2.2 at c = 5 wt % and $n_{e,soln} \approx$ 3.5 at c = 8 wt %. The number of entanglements per chain is given by $n_{e,soln} - 1$ due to the fact that there are always two chains involved in any entanglement. If we define the entanglement concentration as the concentration at which there is an average of one entanglement per chain (i.e., $n_{e,soln}$ = 2), then we can calculate the entanglement concentration for our cellulose sample to be $\phi_c = 2M_e/M \approx 0.046$ or $c_e \approx$ 4.6 wt

dx.doi.org/10.1021/bm300407q | Biomacromolecules XXXX, XXX, XXX−XXX

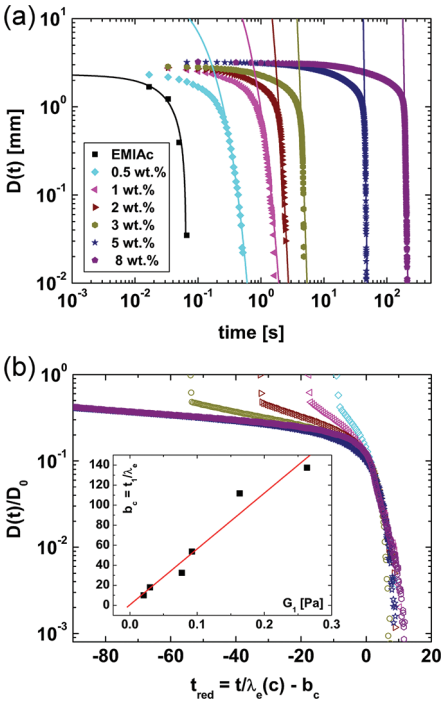

Figure 8. (a) Midfilament diameter as a function of time for cellulose/IL solutions in the CaBER. The data for the Newtonian EMIAc solvent have been fitted with a linear decay (eq 1). The capillary-thinning regions of the cellulose solutions have been fitted with exponential decay functions (eq 2) from which the relaxation times of the solutions have been determined. (b) CaBER master curve generated from the dimensionless midfilament diameter as a function of dimensionless time, $t_{red} = t/\lambda_e\ (c) - b_c$, where $b_c = t_1(c)/\lambda_e(c)$. As shown by the insert, b_c scales with the value of the elastic modulus, G_1, determined from eq 9.

Table 1. Time t_1 at the Onset of the Elastocapillary Thinning Regime in the CaBER Device and Measured Relaxation Times (λ_e) for Cellulose/EMIAc Solutions over a Range of Semidilute Concentrations[a]

c [wt %]	t_1 [s]	λ_e [s]
0.5	0.30	0.03 ± 0.01
1	1.08	0.06 ± 0.01
2	1.95	0.06 ± 0.01
3	4.30	0.08 ± 0.01
5	44.0	0.32 ± 0.04
8	190	1.7 ± 0.2

[a]Values given for λ_e represent the mean and standard deviation over three measurements.

%. Once again this is close to the estimated value of $c_e \approx 10 \times c^*$, obtained from the arguments of Colby.[72]

The relaxation times obtained from the CaBER measurements are shown in Figure 9. They initially increase slowly with concentration and then climb more rapidly in the semidilute and entangled regimes. This growth can be well-described by a simple power law $\lambda_e = 0.046[1 + 0.001(c[\eta])^{3.8}]$. As the concentration tends toward zero, the relaxation time given by this power-law equation approaches a value of $\lambda_0 = 0.046$ s. This is rather higher than our estimate of the Zimm relaxation time ($\lambda_{Zimm} \approx ([\eta]\eta_s M)/(N_A kT)$, where N_A is the Avogadro constant, k is the Boltzmann constant, and T is the temperature), which gives $\lambda_{Zimm} \approx 1$ ms. Such a degree of

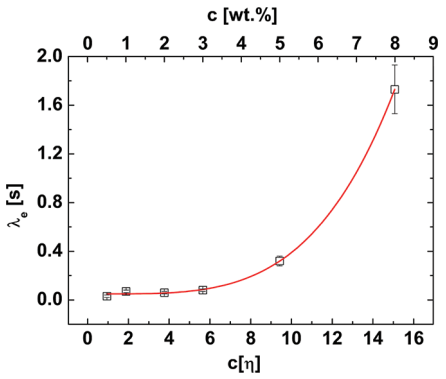

Figure 9. CaBER measured elongational relaxation times (λ_e) as a function of cellulose concentration. The solid red line represents a power-law fit to the data given by $\lambda_e = 0.046[1 + 0.001(c[\eta])^{3.8}]$.

discrepancy is not too surprising because the CaBER device measures the relaxation time of the longest molecules in the (probably) broad molecular weight distribution of the cellulose sample and also because our test fluid concentrations do not extend deeply into the dilute regime.[84] We note that the power-law exponent of 3.8 for λ_e is significantly higher than that found for the concentration dependence of the zero shear viscosity (shown in Figure 3a), which has a power law exponent of 2.4. It has been previously observed that the relaxation time measured using the CaBER can exhibit a stronger concentration dependence compared with shear measurements due to the increased degree of intramolecular interactions induced by chain stretching.[85,86] We note that Arnolds et al.[87] recently reported a weaker dependency of λ_e with concentration for aqueous PEO solutions; however, the high-molecular-weight, flexible PEO chains were in the semidilute entangled and concentrated regimes.

For CaBER experiments at cellulose concentrations $c \geq 3$ wt %, the elastocapillary balance persists for sufficient time that it is possible to use the simple force balance described by eq 6 to estimate the apparent extensional viscosity as a function of the accumulated Hencky strain. As shown in Figure 10a, for 3 and 5 wt % cellulose solutions, we observe only a slight increase in the extensional viscosity with Hencky strain. However, at a concentration of 8 wt % cellulose (corresponding to a concentration sufficient for fiber spinning), the solution displays a more marked increase in η_E from an initially low value to a large plateau value as the Hencky strain increases. Figure 10b shows the corresponding transient Trouton ratio as a function of Hencky strain for the same fluids as Figure 10a. At 3 and 5 wt % cellulose, the Trouton ratio Tr increases with Hencky strain to a limiting value that is only slightly above the Newtonian limit of $Tr = 3$. Only the 8 wt % solution shows a significant increase in Trouton ratio up to a value of $Tr \approx 17$. Whereas this Trouton ratio may seem relatively modest compared with values measured for more flexible polymers, it is a reflection of the limited extensibility of the semiflexible cellulose chains with $L_C/\langle r_0^2\rangle^{1/2} \approx 10$, as discussed above.

DISCUSSION

The intrinsic viscosity $[\eta]$ characterizes the hydrodynamic volume and, although independent of solute concentration, it is affected by the polymer−solvent interactions because these influence the equilibrium coil shape and size.[88−90] The intrinsic viscosity is affected by the rigidity of the chain backbone as well as both molecular weight and molecular weight distribution.[28]

dx.doi.org/10.1021/bm300407q | Biomacromolecules XXXX, XXX, XXX−XXX

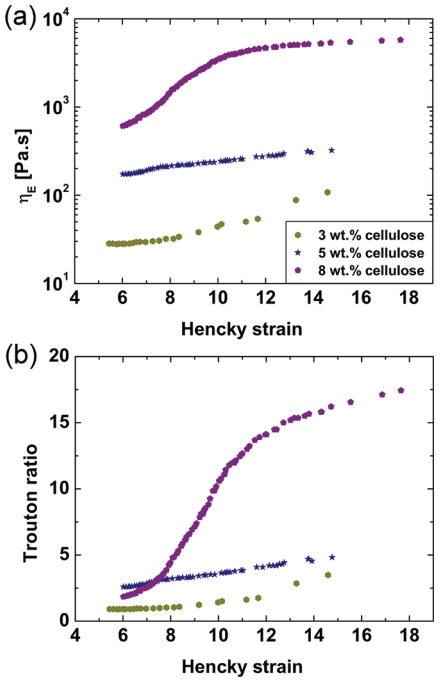

Figure 10. (a) Apparent extensional viscosity and (b) transient Trouton ratio as a function of Hencky strain for cellulose/IL solutions measured in the CaBER.

We computed a value of $[\eta]$ = 188 mL g^{-1} from the concentration dependence of viscosity data, which is very close to the value of $[\eta]$ = 178 mL g^{-1} reported by Gericke et al.[33] for a DP = 1000 cellulose in EMIAc at 20 °C.[27] A higher intrinsic viscosity value of $[\eta]$ = 370 mL g^{-1} is reported for similar molecular weight cellulose dispersed in cuen (copper 2-ethylenediamine) (for cellulose originating as Tercel fibers),[91] and a value of $[\eta]$ = 167 mL g^{-1} is reported for DMAc/LiCl (dimethylacetamide/lithium chloride) at 30 °C.[92] The quality of EMIAc as a solvent for cellulose can be judged by the value of exponent a in the Mark−Houwink−Sakurada (MHS) equation, $[\eta] = K_m M^a$. The MHS equation relates intrinsic viscosity to molecular weight M, and the values of K_m and a reported by Gericke et al.[33] show that EMIAc IL is a theta solvent for cellulose at room temperature, that is, a = 0.5. Our estimate of the overlap concentration, c^*, based on the assumption that EMIAc is a theta solvent for cellulose at room temperature agrees well with the overlap concentration found from the change in dependence of zero-shear rate viscosity on concentration, suggesting that this assumption is valid. Our data indicate that these cellulose/IL solutions are in the dilute limit for $c < c^*$ = 0.5 wt % and are in the semidilute unentangled regime for 0.5 wt % ≤ c ≤ 5 wt %. Despite having only limited data at high concentrations, our viscometric measurements indicate that the solutions enter the semidilute entangled regime for c > 5 wt %, and this is consistent with estimates of the concentration above which the number of entanglements should exceed one per cellulose chain.

The empirical Cox−Merz rule provides a practical means for assessing the presence of any shear-sensitive microstructure in polymer solutions.[5,29] For the case of cellulose dispersed in IL, the agreement between the linear viscoelastic measurements and the steady shear data reported in Figure 2 suggests that the cellulose is dispersed at the molecular level and remains well mixed even under steady shear. A similar conclusion can also be drawn from the intrinsic viscosity measurement as the values obtained for cellulose immersed in EMIAc solvent are similar to the values obtained for DMAc/LiCl solutions, where laser light scattering studies show molecular dispersion (absence of aggregation).[4] In our steady shear tests, the range of shear rates accessible was limited for high cellulose concentrations due to the onset of a rotational instability and ejection of fluid from the rheometer at high shear rates.[93] However, over the range of shear rates that could be tested, the steady shear viscosity overlays the complex viscosity very well, indicating that the empirical Cox−Merz rule holds for these fluids.[94] This is in contrast with the reports of Kuang et al.[37] for cellulose in 1-allyl-3-methylimidazolium chloride (AMICl) and Chen et al.[31] for cellulose in BMICl, who both found that the complex viscosity dropped below the steady shear viscosity at high shear rates. Chen et al. speculate that strong shear could promote intramolecular hydrogen bonding, causing an effective increase in persistence length with shear rate. The fact we do not also observe the failure of the Cox−Merz rule may reflect the fact that ILs containing acetate ions are more effective at dissolving cellulose than those containing chloride, implying that they are more effective at competing for hydrogen bonds.[18]

As previously noted, the elongational kinematics of the fluid jet exiting the spinneret or die in fiber spinning processes is closely approximated by the CaBER. The response of cellulose solutions to uniaxial extensional deformation in the CaBER device has been presented in Figures 8−10. Over a range of semidilute cellulose concentrations, the CaBER data are self-similar in the elastocapillary thinning region, and measurements of the filament diameter versus time can be collapsed onto a master curve by appropriate scaling of the diameter and time axes. We find that the relaxation times of the solutions increase dramatically as the cellulose concentration approaches the fiber spinning concentration regime, that is, as solutions become entangled such that $n_{e,soln} > 2$.[83] The cellulose/EMIAc solutions in this concentration regime display a strain hardening response that is manifested as an increase in the absolute value of the apparent extensional viscosity and an increase in Trouton ratio with increasing Hencky strain. In contrast with the measurements of Sammons et al.,[36] these solutions display extensional hardening, and the value of the transient Trouton ratio or extensional viscosity response is a strong function of both the cellulose concentration and accumulated strain. The strain hardening response of the 8 wt % cellulose solution is conducive to fiber spinning from these solutions. Although the polymer molecular weight is quite high, a relatively large persistence length implies that the extensibility of cellulose chains is low ($L_C/\langle r_0^2\rangle^{1/2} \approx 10$), which helps rationalize the relatively low Trouton ratio for these fluids. The comparison of various polymer solutions in this case shows that the ability of a "spinning dope" to form long, continuous filaments (or "spinnability" as it is often called[95]) increases beyond the entanglement concentration. Consistent with estimates of the minimum solution entanglement number necessary for successful electrospinning of polymer solutions, we estimate an entanglement number of $n_{e,soln} \approx 3.5$ for the 8 wt % cellulose solution.[83] The empirically determined processing parameters used for the spinning of the fibers from 8 wt % cellulose/EMIAc solution shown in Figure 1 (draw ratio DR = 11, strain rate $\dot{\varepsilon} \approx 4$ s^{-1}) are sufficient to generate a high degree of alignment of cellulose chains in the air gap prior to coagulation. The strain rate is high in comparison with the relaxation rate ($1/\lambda_e \approx 0.6$ s^{-1}), and the draw ratio is sufficient to extend

dx.doi.org/10.1021/bm300407q | Biomacromolecules XXXX, XXX, XXX−XXX

significantly the semiflexible cellulose chains. Extensional viscosity and relaxation time measurements made using the CaBER instrument, combined with straightforward estimates of chain extensibility and solution entanglement number, could provide a quick and easy way of characterizing different spinning dopes to determine their suitability for subsequent fiber spinning operations.

As a caveat to the preceding discussion, Ziabicki[95] and others[51,96] have emphasized that apart from rheological properties of spinning dopes, the "spinnability" of fibers from solution also depends on physical and chemical factors that accompany the transition from spinning fluid to a solid spun fiber. These factors include the rate and extent of crystallization, diffusion (solvent removal), cross-linking, gelation, supramolecular structure, association, temperature, composition-dependent phase behavior, and so on.[96,97] The transient extensional viscosity function measured by stretching fluid elements with a free-surface only provides a measure of the strain- and rate- dependence of the viscoelastic stresses generated in the spin-line before material elements enter the coagulation bath. However, high values of the extensional viscosity do help to stabilize the spin-line and provide the potential for spinning at high rates and stretching the filament to high draw ratios and very small diameters. This results in significant axial molecular orientation of the polymer chains before precipitation in the coagulation bath traps and fixes the chains. Because the extent of crystallinity in semicrystalline polymers is related to the degree of orientation, controlling the extension rate during the transition in state from spinning dope to coagulated fiber is necessary for obtaining polymeric filaments with the desired mechanical and physical properties, for example, density, color fastness, microstructure, extent of swelling, shrinkability, and so on.[95−97]

CONCLUSIONS

We have performed a comprehensive study of the shear and extensional rheology of solutions of cellulose dissolved in the room-temperature IL EMIAc. ILs are an emerging class of fluids with potentially important applications for processing of cellulose (and other highly crystalline biopolymers) without requiring derivatization steps involving the use of hazardous chemicals. The viscosity determined from steady shear rheometry in a cone-and-plate rheometer over a wide range of cellulose concentrations spanning the dilute to semidilute regimes was shown to agree well with the complex viscosity determined from linear viscoelasticity measurements, thus satisfying the empirical Cox−Merz rule. This indicates that little disruption to the fluid microstructure is induced by the action of shearing deformations, that is, that the cellulose most likely remains dispersed at the molecular level in the IL solvent and there is no significant aggregation up to concentrations as high as c = 8 wt %. In addition, we have no reason to suspect that shear-induced deformation of the fluid microstructure may lead to cellulose aggregation in our solutions; a mechanism that has been invoked by some previous authors to explain the violation of the Cox−Merz rule.[25,31] Scaling laws for the storage and loss moduli and for the zero-shear viscosity with concentration are consistent with a semiflexible cellulose chain, as expected.

In addition to shear rheology measurements, we present the first observations and measurements of the filament thinning dynamics of cellulose/IL solutions using a capillary thinning extensional rheometer. The CaBER device allows us to observe the thinning and eventual breakup of a fluid filament in a shear-free uniaxial extensional flow, which approximates the deformation experienced by material elements in the air gap between the die and coagulation bath in the dry-jet wet spinning process. When the cellulose solutions enter the elastocapillary thinning regime, measurements of the midfilament diameter as a function of time in the CaBER device allow direct determination of the dominant fluid relaxation time controlling chain stretching in the fluid as well as the growth in the transient extensional stress in the filament due to the elongation of cellulose chains. We find that as cellulose concentrations exceed the entanglement limit and approach those used for fiber spinning, there is a significant increase in the characteristic fluid relaxation time $\lambda_e(c)$. The transient extensional viscosity concomitantly exhibits a significant increase with Hencky strain that is absent at lower concentrations, and this strain hardening can help stabilize the viscoelastic spinline that constitutes a central part of the cellulose fiber formation process.

ASSOCIATED CONTENT

Supporting Information

Results of ^{1}H NMR spectroscopy performed on our EMIAc sample to confirm its purity and results of cone-and-plate shear rheometry performed on a solution of cellulose in EMIAc over an extended time period, the results of which indicate that degradation of cellulose subsequent to dissolution can be neglected on the time scale of the rheology experiments presented in the main article. This material is available free of charge via the Internet at http://pubs.acs.org.

AUTHOR INFORMATION

Corresponding Author

*Tel: +1 6172530273; E-mail: shaward@mit.edu (S.J.H.). Tel: +44 117 3315330; E-mail: Sameer.Rahatekar@bristol.ac.uk (S.S.R.).

Notes

The authors declare no competing financial interest.

ACKNOWLEDGMENTS

G.H.M. and S.J.H. acknowledge NASA Microgravity Fluid Sciences (Code UG) for support of this research under grant NNX09AV99G. V.S. acknowledges AkzoNobel for financial support. S.S.R. acknowledges financial support from the Faculty of Engineering, University of Bristol.

REFERENCES

(1) Klemm, D.; Heublein, B.; Fink, H. P.; Bohn, A. Cellulose: fascinating biopolymer and sustainable raw material. *Angew. Chem., Int. Ed.* **2005**, *44* (22), 3358−3393.

(2) Kamide, K. *Cellulose and Cellulose Derivatives: Molecular Characterization and Its Applications*; Elsevier: Amsterdam, 2005.

(3) Ott, E. *Cellulose and Cellulose Derivatives*; Interscience Publishers: New York, 1943; Vol. *V*.

(4) Dumitriu, S. *Polysaccharides: Structural Diversity and Functional Versatility*, 2nd ed.; Marcel Dekker: New York, 2005.

(5) Lapasin, R.; Pricl, S. *Rheology of Industrial Polysaccharides: Theory and Applications*; Chapman & Hall: London, 1995.

(6) Hamad, W. *Cellulosic Materials: Fibers, Networks and Composites*; Kluwer Academic Publishers: Boston, 2002.

(7) Hermanutz, F.; Gahr, F.; Uerdingen, E.; Meister, F.; Kosan, B. New developments in dissolving and processing of cellulose in ionic liquids. *Macromol. Symp.* **2008**, *262*, 23−27.

(8) Woodings, C. *Regenerated Cellulose Fibres*; Woodhead Publishing Limited: Cambridge, 2001.
(9) Pinkert, A.; Marsh, K. N.; Pang, S. S.; Staiger, M. P. Ionic liquids and their interaction with cellulose. *Chem. Rev.* **2009**, *109* (12), 6712−6728.
(10) Zhu, S.; Wu, Y.; Chen, Q.; Yu, Z.; Wang, C.; Jin, S.; Ding, Y.; Wu, G. Dissolution of cellulose with ionic liquids and its application: a mini-review. *Green Chem.* **2006**, *8*, 325−327.
(11) Wendler, F.; Kosan, B.; Krieg, M.; Meister, F. Possibilities for the physical modification of cellulose shapes using ionic liquids. *Macromol. Symp.* **2009**, *280*, 112−122.
(12) Swatloski, R. P.; Spear, S. K.; Holbrey, J. D.; Rogers, R. D. Dissolution of cellulose with ionic liquids. *J. Am. Chem. Soc.* **2002**, *124*, 4974−4975.
(13) Viswanathan, G.; Murugesan, S.; Pushparaj, V.; Nalamasu, O.; Ajayan, P. M.; Linhardt, R. J. Preparation of biopolymer fibers by electrospinning from room temperature ionic liquids. *Biomacromolecules* **2006**, *7* (2), 415−418.
(14) Phillips, D. M.; Drummy, L. F.; Conrady, D. G.; Fox, D. M.; Naik, R. R.; Stone, M. O.; Trulove, P. C.; De Long, H. C.; Mantz, R. A. Dissolution and regeneration of *Bombyx mori* silk fibroin using ionic liquids. *J. Am. Chem. Soc.* **2004**, *126* (44), 14350−14351.
(15) Xie, H. B.; Li, S. H.; Zhang, S. B. Ionic liquids as novel solvents for the dissolution and blending of wool keratin fibers. *Green Chem.* **2005**, *7* (8), 606−608.
(16) Xie, H.; Zhang, S.; Li, S. Chitin and chitosan dissolved in ionic liquids as reversible sorbents of CO_2. *Green Chem.* **2006**, *8* (7), 630−633.
(17) Qin, Y.; Lu, X.; Sun, N.; Rogers, R. D. Dissolution or extraction of crustacean shells using ionic liquids to obtain high molecular weight purified chitin and direct production of chitin films and fibers. *Green Chem.* **2010**, *12*, 968−971.
(18) Sun, N.; Rahman, M.; Qin, Y.; Maxim, M. L.; Rodriguez, H.; Rogers, R. D. Complete dissolution and partial delignification of wood in the ionic liquid 1-ethyl-3-methylimidazolium acetate. *Green Chem.* **2009**, *11*, 646−655.
(19) Sun, N.; Rodriguez, H.; Rahman, M.; Rogers, R. D. Where are ionic liquid strategies most suited in the pursuit of chemicals and energy from lignocellulosic biomass? *Chem. Commun.* **2011**, *47*, 1405−1421.
(20) Brandt, A.; Ray, M. J.; To, T. Q.; Leak, D. J.; Murphy, R. J.; Welton, T. Ionic liquid pretreatment of lignocellulosic biomass with ionic liquid-water mixtures. *Green Chem.* **2011**, *13*, 2489−2499.
(21) Schrems, M.; Brandt, A.; Welton, T.; Liebner, F.; Rosenau, T.; Potthast, A. Ionic liquids as media for biomass processing: opportunities and restrictions. *Holzforschung* **2011**, *65*, 527−533.
(22) Fox, D. M.; Awad, W. H.; Gilman, J. W.; Maupin, P. H.; De Long, H. C.; Trulove, P. C. Flammability, thermal stability, and phase change characteristics of several trialkylimidazolium salts. *Green Chem.* **2003**, *5*, 724−727.
(23) Shill, K.; Padmanabhan, S.; Xin, Q.; Prausnitz, J. M.; Clark, D. S.; Blanch, H. W. Ionic liquid pretreatment of cellulosic biomass: enzymatic hydrolysis and ionic liquid recycle. *Biotechnol. Bioeng.* **2011**, *108* (3), 511−520.
(24) Ueki, T.; Watanabe, M. Macromolecules in ionic liquids: Progress, challenges, and opportunities. *Macromolecules* **2008**, *41* (11), 3739−3749.
(25) Lodge, T. P. Materials science - a unique platform for materials design. *Science* **2008**, *321* (5885), 50−51.
(26) Lu, J. M.; Yan, F.; Texter, J. Advanced applications of ionic liquids in polymer science. *Prog. Polym. Sci.* **2009**, *34* (5), 431−448.
(27) Zhang, J.; Zhang, H.; Wu, J.; Zhang, J.; He, J.; Xiang, J. NMR spectroscopic studies of cellobiose solvation in EmimAc aimed to understand the dissolution mechanism of cellulose in ionic liquids. *Phys. Chem. Chem. Phys.* **2010**, *12*, 1941−1947.
(28) Graessley, W. W. *Polymeric Liquids and Networks: Structure and Properties*; Taylor and Francis Group: New York, 2004.
(29) Larson, R. G. *The Structure and Rheology of Complex Fluids*; Oxford University Press: New York, 1999.
(30) Horinaka, J.-i.; Yasuda, R.; Takigawa, T. Entanglement properties of cellulose and amylose in an ionic liquid. *J. Polym. Sci., Part B: Polym. Phys.* **2011**, *49*, 961−965.
(31) Chen, X.; Zhang, Y.; Wang, H.; Wang, S.-W.; Liang, S.; Colby, R. H. Solution rheology of cellulose in 1-butyl-3-methyl imidazolium chloride. *J. Rheol.* **2011**, *55* (3), 485−494.
(32) Chen, X.; Zhang, Y. M.; Cheng, L. Y.; Wang, H. P. Rheology of concentrated cellulose solutions in 1-butyl-3-methylimidazolium chloride. *J. Polym. Environ.* **2009**, *17*, 273−279.
(33) Gericke, M.; Schlufter, K.; Liebert, T.; Heinze, T.; Budtova, T. Rheological properties of cellulose/ionic liquid solutions: from dilute to concentrated states. *Biomacromolecules* **2009**, *10* (5), 1188−1194.
(34) Collier, J. R.; Watson, J. L.; Collier, B. J.; Petrovan, S. Rheology of 1-butyl-3-methylimidazolium chloride cellulose solutions. II. Solution character and preparation. *J. Appl. Polym. Sci.* **2009**, *111*, 1019−1027.
(35) Sammons, R. J.; Collier, J. R.; Rials, T. G.; Petrovan, S. Rheology of 1-butyl-3-methylimidazolium chloride cellulose solutions. I. Shear rheology. *J. Appl. Polym. Sci.* **2008**, *110*, 1175−1181.
(36) Sammons, R. J.; Collier, J. R.; Rials, T. G.; Petrovan, S. Rheology of 1-butyl-3-methylimidazolium chloride cellulose solutions. III. Elongational rheology. *J. Appl. Polym. Sci.* **2008**, *110*, 3203−3208.
(37) Kuang, Q.-L.; Zhao, J.-C.; Niu, Y.-H.; Zhang, J.; Wang, Z.-G. Celluloses in an ionic liquid: the rheological properties of the solutions spanning the dilute and semidilute regimes. *J. Phys. Chem. B* **2008**, *112*, 10234−10240.
(38) McKinley, G. H. Visco-elasto-capillary thinning and break-up of complex fluids. In *Rheology Reviews*; British Society of Rheology: Aberystwyth, 2005; pp 1−48.
(39) McKinley, G. H.; Sridhar, T. Filament-stretching rheometry of complex fluids. *Annu. Rev. Fluid Mech.* **2002**, *34*, 375−415.
(40) Zugenmaier, P. Contribution to the historical development of macromolecular chemistry - exemplified on cellulose. *Cellul. Chem. Technol.* **2009**, *43* (9−10), 351−378.
(41) Mark, H.; Tobolsky, A. V. *Physical Chemistry of High Polymeric Systems*, 2nd ed.; Interscience Publishers: New York, 1950; Vol. *II*.
(42) Mulhaupt, R. Hermann Staudinger and the origin of macromolecular chemistry. *Angew. Chem., Int. Ed.* **2004**, *43* (9), 1054−1063.
(43) Cai, T.; Zhang, H.; Guo, Q.; Shao, H.; Hu, X. Structure and properties of cellulose fibers from ionic liquids. *J. Appl. Polym. Sci.* **2010**, *115* (2), 1047−1053.
(44) Rahatekar, S. S.; Rasheed, A.; Jain, R.; Zammarano, M.; Koziol, K. K.; Windle, A. H.; Gilman, J. W.; Kumar, S. Solution spinning of cellulose carbon nanotube composites using room temperature ionic liquids. *Polymer* **2009**, *50*, 4577−4583.
(45) Zhang, H.; Wang, Z. G.; Zhang, Z. N.; Wu, J.; Zhang, J.; He, J. S. Regenerated-cellulose/multiwalled- carbon-nanotube composite fibers with enhanced mechanical properties prepared with the ionic liquid 1-allyl-3-methylimidazolium chloride. *Adv. Mater.* **2007**, *19* (5), 698−704.
(46) Sun, N.; Swatloski, R. P.; Maxim, M. L.; Rahman, M.; Harland, A. G.; Haque, A.; Spear, S. K.; Daly, D. T.; Rogers, R. D. Magnetite-embedded cellulose fibers prepared from ionic liquid. *J. Mater. Chem.* **2008**, *18*, 283−290.
(47) Denn, M. M. Continuous drawing of liquids to form fibers. *Annu. Rev. Fluid Mech.* **1980**, *12*, 365−387.
(48) Rajagopalan, D. Computational analysis of techniques to determine extensional viscosity from entrance flows. *Rheol. Acta* **2000**, *39* (2), 138−151.
(49) Sescousse, R.; Le, K. A.; Ries, M. E.; Budtova, T. Viscosity of cellulose−imidazolium-based ionic liquid solutions. *J. Phys. Chem. B* **2010**, *114*, 7222−7228.
(50) Entov, V. M.; Hinch, E. J. Effect of a spectrum of relaxation times on the capillary thinning of a filament of elastic liquid. *J. Non-Newtonian Fluid Mech.* **1997**, *72*, 31−54.
(51) Petrie, C. J. S. *Elongational Flows*; Pitman: London, 1979.
(52) Petrie, C. J. S. Extensional viscosity: a critical discussion. *J. Non-Newtonian Fluid Mech.* **2006**, *137* (1−3), 15−23.

(53) Vitz, J.; Erdmenger, T.; Haensch, C.; Schubert, U. S. Extended dissolution studies of cellulose in imidazolium based ionic liquids. *Green Chem.* **2009**, *11*, 417−424.
(54) Bentivoglio, G.; Roder, T.; Fasching, M.; Buchberger, M.; Schottenberger, H.; Sixta, H. Cellulose processing with chloride-based ionic liquids. *Lenzinger Ber.* **2006**, *86*, 154−161.
(55) Zhang, H.; Wu, J.; Zhang, J.; He, J. 1-Allyl-3-methylimidazolium chloride room temperature ionic liquid: a new and powerful nonderivatizing solvent for cellulose. *Macromolecules* **2005**, *38*, 8272−8277.
(56) Rinaldi, R.; Palkovits, R.; Schuth, F. Depolymerization of cellulose using solid catalysts in ionic liquids. *Angew. Chem., Int. Ed.* **2008**, *47* (42), 8047−8050.
(57) Watanabe, H. The study of factors influencing the depolymerisation of cellulose using a solid catalyst in ionic liquids. *Carbohydr. Polym.* **2010**, *80* (4), 1168−1171.
(58) Sievers, C.; Valenzuela-Olarte, M. B.; Marzialetti, T.; Musin, I.; Agrawal, P. K.; Jones, C. W. Ionic-liquid-phase hydrolysis of pine wood. *Ind. Eng. Chem. Res.* **2009**, *48* (3), 1277−1286.
(59) Amarasekara, A. S.; Wiredu, B. Degradation of cellulose in dilute aqueous solutions of acidic ionic liquid 1-(1-propylsulfonic)-3-methylimidazolium chloride, and *p*-toluenesulfonic acid at moderate temperatures and pressures. *Ind. Eng. Chem. Res.* **2011**, *50* (21), 12276−12280.
(60) Kosan, B.; Schwikal, K.; Meister, F. Solution states of cellulose in selected direct dissolution agents. *Cellulose* **2010**, *17*, 495−506.
(61) Stelter, M.; Brenn, G. Validation and application of a novel elongational device for polymer solutions. *J. Rheol.* **2000**, *44* (3), 595−616.
(62) Wang, M.; Yu, J. H.; Kaplan, D. L.; Rutledge, G. C. Production of submicron diameter silk fibers under benign processing conditions by two-fluid electrospinning. *Macromolecules* **2006**, *39*, 1102−1107.
(63) Duxenneuner, M. R.; Fischer, P.; Windhab, E. J.; Cooper-White, J. J. Extensional properties of hydroxypropyl ether guar gum solutions. *Biomacromolecules* **2008**, *9* (11), 2989−2996.
(64) David, R. L. A.; Wei, M. H.; Liu, D.; Bathel, B. F.; Plog, J. P.; Ratner, A.; Kornfield, J. A. Effects of pairwise, self-associating functional side groups on polymer solubility, solution viscosity, and mist control. *Macromolecules* **2009**, *42* (4), 1380−1391.
(65) Rodd, L. E.; Scott, T. P.; Cooper-White, J. J.; McKinley, G. H. Capillary break-up rheometry of low-viscosity elastic fluids. *Appl. Rheol.* **2005**, *15* (1), 12−27.
(66) Papageorgiou, D. T. On the breakup of viscous liquid threads. *Phys. Fluids* **1995**, *7*, 1529−1544.
(67) McKinley, G. H.; Tripathi, A. How to extract the Newtonian viscosity from capillary breakup measurements in a filament rheometer. *J. Rheol.* **2000**, *44* (3), 653−670.
(68) Anna, S. L.; McKinley, G. H. Elasto-capillary thinning and breakup of model elastic liquids. *J. Rheol.* **2001**, *45* (1), 115−138.
(69) Cox, W. P.; Merz, E. H. Correlation of dynamic and steady flow viscosities. *J. Polym. Sci.* **1958**, *28* (118), 619−622.
(70) Gonsior, N.; Hetzer, M.; Kulicke, W.-M.; Ritter, H. First studies on the influence of methylated *β*-cyclodextrin on the rheological behavior of 1-ethyl-3-methyl imidazolium acetate. *J. Phys. Chem. B* **2010**, *114*, 12468−12472.
(71) Fendt, S.; Padmanabhan, S.; Blanch, H. W.; Prausnitz, J. M. Viscosities of acetate or chloride-based ionic liquids and some of their mixtures with water or other common solvents. *J. Chem. Eng. Data* **2011**, *56*, 31−34.
(72) Colby, R. H. Structure and linear viscoelasticity of flexible polymer solutions: comparison of polyelectrolyte and neutral polymer solutions. *Rheol. Acta* **2010**, *49*, 425−442.
(73) Kulicke, W.-M.; Kniewske, R. The shear viscosity dependence on concentration, molecular weight and shear rate of polystyrene solutions. *Rheol. Acta* **1984**, *23*, 75−83.
(74) Colby, R. H.; Rubinstein, M. Two-parameter scaling for polymers in theta solvents. *Macromolecules* **1990**, *23*, 2753−2757.
(75) Song, H.; Niu, Y.; Wang, Z.; Zhang, J. Liquid crystalline phase and gel-sol transitions for concentrated microcrystalline cellulose (MCC)/1-ethyl-3-methylimidazolium acetate (EMIMAc) solutions. *Biomacromolecules* **2011**, *12* (4), 1087−1096.
(76) Flory, P. J.; Fox, T. G. Treatment of intrinsic viscosities. *J. Am. Chem. Soc.* **1951**, *73* (5), 1904−1908.
(77) Flory, P. J.; Spurr, O. K. J.; Carpenter, D. K. Intrinsic viscosities of cellulose derivatives. *J. Polym. Sci.* **1958**, *27*, 231−240.
(78) Saalwachter, K.; Burchard, W.; Klufers, P.; Kettenbach, G.; Mayer, P.; Klemm, D.; Dugarmaa, S. Cellulose solutions in water containing metal complexes. *Macromolecules* **2000**, *33* (11), 4094−4107.
(79) Graessley, W. W. Polymer chain dimensions and the dependence of viscoelastic properties on concentration, molecular weight and solvent power. *Polymer* **1980**, *21*, 258−262.
(80) Graessley, W. W. Linear viscoelasticity in entangling polymer systems. *J. Chem. Phys.* **1971**, *54* (12), 5143−5157.
(81) Morse, D. C. Viscoelasticity of tightly entangled solutions of semiflexible polymers. *Phys. Rev. E* **1998**, *58* (2), R1237−R1240.
(82) Koenderink, G. H.; Atakhorrami, M.; MacKintosh, F. C.; Schmidt, C. F. High-frequency stress relaxation in semiflexible polymer solutions and networks. *Phys. Rev. Lett.* **2006**, *96*, 138307.
(83) Shenoy, S. L.; Bates, W. D.; Frisch, H. L.; Wnek, G. E. Role of chain entanglements on fiber formation during electrospinning of polymer solutions: good solvent, non-specific polymer-polymer interaction limit. *Polymer* **2005**, *46*, 3372−3384.
(84) Rodd, L. E.; Cooper-White, J. J.; Boger, D. V.; McKinley, G. H. Role of the elasticity number in the entry flow of dilute polymer solutions in micro-fabricated contraction geometries. *J. Non-Newtonian Fluid Mech.* **2007**, *143* (2−3), 170−191.
(85) Clasen, C.; Plog, J. P.; Kulicke, W. M.; Owens, M.; Macosko, C.; Scriven, L. E.; Verani, M.; McKinley, G. H. How dilute are dilute solutions in extensional flows? *J. Rheol.* **2006**, *50* (6), 849−881.
(86) Tirtaatmadja, V.; McKinley, G. H.; Cooper-White, J. J. Drop formation and breakup of low viscosity elastic fluids: effects of molecular weight and concentration. *Phys. Fluids* **2006**, *18* (4), 043101.
(87) Arnolds, O.; Buggisch, H.; Sachsenheimer, D.; Willenbacher, N. Capillary breakup extensional rheometry (CaBER) on semi-dilute and concentrated polyethyleneoxide (PEO) solutions. *Rheol. Acta* **2010**, *49*, 1207−1217.
(88) Harding, S. E. The intrinsic viscosity of biological macromolecules. Progress in measurement, interpretation and application to structure in dilute solution. *Prog. Biophys. Mol. Biol.* **1997**, *68* (2−3), 207−262.
(89) Flory, P. J. *Principles of Polymer Chemistry*; Cornell University Press: Ithaca, 1953.
(90) Doi, M.; Edwards, S. F. *The Theory of Polymer Dynamics*; Oxford University Press: New York, 1988.
(91) Eckelt, J.; Knopf, A.; Roder, T.; Weber, H. K.; Sixta, H.; Wolf, B. A. Viscosity-molecular weight relationship for cellulose solutions in either NMMO monohydrate or cuen. *J. Appl. Polym. Sci.* **2011**, *119* (2), 670−676.
(92) McCormick, C. L.; Callais, P. A.; Hutchinson, B. H. Solution studies of cellulose in lithium chloride and *N*,*N*-dimethylacetamide. *Macromolecules* **1985**, *18* (12), 2394−2401.
(93) Pipe, C. J.; Majmudar, T. S.; McKinley, G. H. High shear rate viscometry. *Rheol. Acta* **2008**, *47* (5−6), 621−642.
(94) Bird, R. B.; Armstrong, R. C.; Hassager, O. *Dynamics of Polymeric Liquids*, 2nd ed.; John Wiley & Sons: New York, 1987; Vol. *1*.
(95) Ziabicki, A. *Fundamentals of Fibre Formation*; John Wiley & Sons: New York, 1976.
(96) Mark, H. F.; Atlas, S. M.; Cernia, E. *Man Made Fibers: Science and Technology*; John Wiley & Sons: New York, 1967; Vol. *1*.
(97) Gupta, V. B.; Kothari, V. K. *Manufactured Fiber Technology*; Chapman & Hall: London, 1997.